2013 European Control Conference (ECC)
July 17-19, 2013, Zürich, Switzerland.

A spectral estimation case study in frequency-domain by subspace methods

Hüseyin Akçay and Semiha Türkay
Department of Electrical and Electronics Engineering, Anadolu University
Eskisehir 26470, Turkey

***Abstract*— In this paper, the properties of two recently proposed frequency-domain subspace-based algorithms to estimate discrete-time cross-power spectral density (cross-PSD) and auto-power spectral density (auto-PSD) matrices of vector auto-regressive moving-average and moving-average (ARMAMA) models from sampled values of the Welch cross-PSD and auto-PSD estimators on uniform grids of frequencies, are illustrated by numerical and real-life application examples. The latter is concerned with the modeling of acoustic spectra for detecting faults in induction motors.**

***Index Terms*— power spectrum, subspace identification, Welch estimator, dynamic factor model, acoustic spectra.**

I. Introduction

The cross-spectral analysis is a fundamental and powerful technique to investigate an unknown relationship between two time series in frequency-domain. It is widely used in many engineering problems; e.g., time delay estimation of spatial sensors [1], [2], blind equalization in communications [3], speech enhancement [4], analysis of feedback systems [5], system identification of mechanical vibration systems [6], atmospheric problems [7], and vibration testing of structures against earthquake and wind loads [8].

The cross-PSD function has mostly been computed in a nonparametric way by using the fast Fourier transform (FFT). A parametric approach was recently proposed in [9] for the cross-spectral analysis of the so–called ARMAMA models. See Section 2, for the definition of vector ARMAMA models.

In [10], the cross-PSD and the auto-PSD matrices were estimated by subspace methods using the averaged periodograms (the Welch auto and cross-PSD estimates) computed on uniform grids of frequencies from observed time series. The proposed algorithms are realization based and the AR parameters are computed by Hankel matrix factorization followed by extraction of the so-called observability range space, and the MA parameters are estimated from the data by a least-squares procedure. An additional step, which is implemented as solution to a convex semidefinite programming problem, comes into action when the lack of positivity of the estimated auto-PSD has been detected.

The purpose of this paper is to illustrate in a case study the properties of the identification algorithms developed in [10] by means of numerical and real-life application examples. The latter is concerned with the modeling of acoustic spectra for detecting faults in induction motors.

II. The Vector ARMAMA Model

Let $x[k] \in \mathbf{R}^{m_x}$ and $y[k] \in \mathbf{R}^{m_y}$ be observable output sequences of two jointly stationary processes. The discrete-time vector ARMAMA model is defined as

$$x[k] = G_x(z)e[k] + H_x(z)e_x[k], \quad (1)$$
$$y[k] = G_y(z)e[k] + H_y(z)e_y[k] \quad (2)$$

where $e[k] \in \mathbf{R}^{m_e}$, $e_x[k] \in \mathbf{R}^{\nu_x}$, and $e_y[k] \in \mathbf{R}^{\nu_y}$ are unobservable inputs of white-noise sequences with zero-means and unit covariance matrices, which are mutually independent; $G_x(z), G_y(z), H_x(z), H_y(z)$ have MacMillan degrees respectively $n_x, n_y, \kappa_x, \kappa_y$ and their poles are inside the unit circle; $H_x(z)$ and $H_y(z)$ are proper and minimum phase; $G_x(z)$ and $G_y(z)$ are strictly proper, minimum phase, and have neither poles nor zeros at the origin. The block diagram of the vector ARMAMA model is shown in Figure 1.

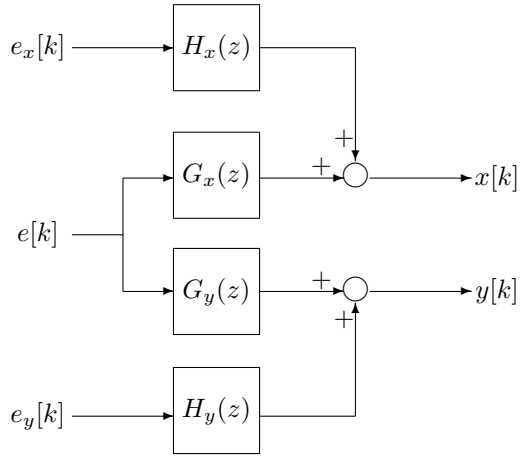

Fig. 1. Block diagram of the ARMAMA model.

The model defined by Eqs. (1) and (2) is actually a very special case of the *dynamic factor model* [11], [12] or *errors-in-variables model* [13].

III. The Welch method

Welch introduced a method [14] that is particularly well suited to direct computation of a power spectrum estimator using the FFT. In his method, a data record $x[k], 0 \leq k < N$

is divided into L disjoint segments of M samples each so that $N = LM$, i.e., the segments

$$x^{(i)}[k] = x[k + iM], \qquad 0 \le k < M, \;\; 0 \le i < L \tag{3}$$

are formed and the modified periodograms

$$S_{xx}^{(i)}(\omega; M) \;\; = \;\; \frac{1}{M} X_{(i)}^T(\omega; M) X_{(i)}(-\omega; M) \tag{4}$$

are computed for $i = 0, \cdots, L-1$ where

$$X_{(i)}(\omega; M) = \sum_{n=0}^{M-1} x^{(i)}[n] e^{-j\omega n}. \tag{5}$$

The Welch auto-PSD estimator is then defined as

$$S_{xx}^W(e^{j\omega}) = \frac{1}{L} \sum_{i=0}^{L-1} S_{xx}^{(i)}(\omega; M). \tag{6}$$

The Welch cross-PSD estimator of two random signals $x[k]$ and $y[k]$ is defined as

$$S_{xy}^W(e^{j\omega}) = \frac{1}{L} \sum_{i=0}^{L-1} S_{xy}^{(i)}(\omega; M) \tag{7}$$

where

$$S_{xy}^{(i)}(\omega; M) = \frac{1}{M} X_{(i)}^T(\omega; M) Y_{(i)}(-\omega; M) \tag{8}$$

and $Y_{(i)}(\omega; M)$ is defined similarly to Eq. (5).

IV. The spectral estimation problems

In this paper, in a case study we study applications of the following estimation problems.

Problem 4.1 (Cross-PSD Estimation):
Given: the samples of the Welch cross-PSD estimator

$$S_{xy}^W(e^{j\frac{2\pi n}{M}}), \qquad n = 0, \cdots, M/2, \tag{9}$$

Find: a strongly consistent estimator $\widehat{S}_{xy}(z)$ of the cross-PSD matrix $S_{xy}(z) = G_x(z) G_y^T(z^{-1})$.

We will restrict the attention to finding the state-space parameters of $S_{xy}(z)$. Unless both $G_x(z)$ and $G_y(z)$ are scalar functions, their parameters can not be determined solely from $S_{xy}(z)$ as discussed in [10].

Problem 4.2 (Auto-PSD Estimation):
Given: the samples of the Welch auto-PSD estimator

$$S_{xx}^W(e^{j\frac{2\pi n}{M}}), \qquad n = 0, \cdots, M/2 \tag{10}$$

where $x = G_x(z)e$ and $G_x(z)$ is proper,
Find: a minimum-phase stable factor $\widehat{G}_x(z)$ such that $\widehat{S}_{xx}(z) = \widehat{G}_x(z) \widehat{G}_x^T(z^{-1})$ is a strongly consistent estimator of the auto-PSD matrix $S_{xx}(z) = G_x(z) G_x^T(z^{-1})$.

The problem of determining all of the transfer functions $G_x(z), G_y(z), H_x(z), H_y(z)$ from the sampled values of the auto-PSD and the cross-PSD matrices of $x[k]$ and $y[k]$ is not treated in this paper. This topic is left as a future study.

V. Estimation of the cross-PSD and the auto-PSD matrices by subspace methods

In this section, we review the subspace algorithms developed in [10] which consistently estimate the cross-PSD and the auto-PSD matrices from the samples in Eqs. (9) and (10).

Algorithm 5.1 (Cross-PSD Estimation Algorithm):

1) Expand the Welch cross-PSD samples in Eq. (9) according to the relation $S_{xy}^W(e^{-j\omega}) = \overline{S_{xy}^W(e^{j\omega})}$ to obtain samples of lengths M.
2) Fix the parameters p and r as $p > n_x + n_y$, $r \ge n_x + n_y$, $p + r \le M$ and for $k = 1, \cdots, p$; $l = 1, \cdots, r$, compute the Hankel matrix $\mathcal{Y}$ defined blockwise by

$$\mathcal{Y}_{kl} = \hat{s}_{xy}[k+l-1] + \hat{s}_{xy}[M+k+l-p-r-1] \tag{11}$$

where for $k = 0, \cdots, M-1$, with $z_k = e^{j\frac{2\pi k}{M}}$,

$$\hat{s}_{xy}[k] = \frac{1}{M} \sum_{n=0}^{M-1} z_n^k \, S_{xy}^W(z_n). \tag{12}$$

3) Calculate the SVD

$$\mathcal{Y} = \begin{bmatrix} U^\sharp & U' \end{bmatrix} \begin{bmatrix} \Sigma^\sharp & 0 \\ 0 & \Sigma' \end{bmatrix} \begin{bmatrix} V^\sharp \\ V' \end{bmatrix} \tag{13}$$

where this decomposition is partitioned such that $\Sigma^\sharp$ contains the $n_x + n_y$ largest singular values.
4) With $U^\sharp$ defined by Eq. (13) and $J_{\rm u}$ and $J_{\rm d}$ by

$$J_{\rm u} \;\; = \;\; \begin{bmatrix} 0_{(p-1)m_x \times m_x} & I_{(p-1)m_x} \end{bmatrix}, \tag{14}$$

$$J_{\rm d} \;\; = \;\; \begin{bmatrix} I_{(p-1)m_x} & 0_{(p-1)m_x \times m_x} \end{bmatrix}, \tag{15}$$

calculate

$$A^\sharp \;\; = \;\; (J_{\rm d} U^\sharp)^\dagger J_{\rm u} U^\sharp. \tag{16}$$

5) Put $A^\sharp$ into the following canonical form:

$$A^\sharp = \begin{bmatrix} \Pi_{\rm c} & \Pi_{\rm ac} \end{bmatrix} \begin{bmatrix} \Sigma_{\rm c} & 0 \\ 0 & \Sigma_{\rm ac} \end{bmatrix} \begin{bmatrix} \Pi_{\rm c} & \Pi_{\rm ac} \end{bmatrix}^{-1}$$

where the eigenvalues of $\Sigma_{\rm c}$ are inside the unit circle and the eigenvalues of $\Sigma_{\rm ac}$ are outside the unit circle and let

$$\widehat{A}_{\rm c} \;\; = \;\; \Sigma_{\rm c}, \qquad \widehat{C}_{\rm c} = J_{\rm f} U^\sharp \Pi_{\rm c}, \tag{17}$$

$$\widehat{A}_{\rm ac} \;\; = \;\; \Sigma_{\rm ac}^{-1}, \qquad \widehat{C}_{\rm ac} = J_{\rm l} U^\sharp \Pi_{\rm ac}, \tag{18}$$

where

$$J_{\rm f} \;\; = \;\; \begin{bmatrix} I_{m_x} & 0_{m_x \times (p-1)m_x} \end{bmatrix}, \tag{19}$$

$$J_{\rm l} \;\; = \;\; \begin{bmatrix} 0_{m_x \times (p-1)m_x} & I_{m_x} \end{bmatrix}. \tag{20}$$

6) For the estimates of E, $B_{\rm c}$ and $B_{\rm ac}$, solve the linear least-squares problem:

$$\min_{\widehat{E}, \widehat{B}_{\rm c}, \widehat{B}_{\rm ac}} \sum_{n=0}^{M-1} \left\| S_{xy}^W(z_n) - E - \chi(z_n) \begin{bmatrix} \widehat{B}_{\rm c} \\ \widehat{B}_{\rm ac} \end{bmatrix} \right\|_F^2$$

where $\chi(z) = \begin{bmatrix} C_{\rm c}(zI - A_c)^{-1} & C_{\rm ac}(z^{-1}I - A_{ac})^{-1} \end{bmatrix}$.

7) As the estimator of $S_{xy}(z)$, set

$$\begin{aligned}\widehat{S}_{xy}(z) &= \widehat{E} + \widehat{C}_{\rm c}(zI - \widehat{A}_{\rm c})^{-1}\widehat{B}_{\rm c} \\ &\quad + \widehat{C}_{\rm ac}(z^{-1}I - \widehat{A}_{\rm ac})^{-1}\widehat{B}_{\rm ac}.\end{aligned} \tag{21}$$

Algorithm 5.2 (Auto-PSD Estimation Algorithm):

1) Replace $S^W_{xy}(z_n)$ with $S^W_{xx}(z_n)$ in Algorithm 5.1 and set $n_x = n_y$, $m_x = m_y$. Repeat steps 1–5 of Algorithm 5.1 and compute $\widehat{A}_{\rm c}$ and $\widehat{C}_{\rm c}$ from Eq. (17).
2) Solve the linear least-squares problem:

$$\min_{\widehat{E},\widehat{F}} \sum_{n=0}^{M-1} \left\| \widetilde{\chi}(z_n)\widehat{F} + \widehat{F}^T\widetilde{\chi}^H(z_n) + \widehat{E} - S^W_{xy}(z_n) \right\|_F^2$$

where $\widetilde{\chi}(z) = \widehat{C}_{\rm c}(zI_{n_x} - \widehat{A}_{\rm c})^{-1}$.
3) If $\widehat{H}(z) = \frac{\widehat{E}}{2} + \widehat{C}_{\rm c}(zI_{n_x} - \widehat{A}_{\rm c})\widehat{F}$ is not positive real, solve the linear matrix inequality problem:

$$\min_{\widetilde{E},\widetilde{F},P} \|\widehat{H} - \widetilde{H}\|_2 \tag{22}$$

subject to the constraints

$$\widehat{\mathcal{M}}(\widetilde{E},\widetilde{F}) = \begin{bmatrix} P - \widehat{A}_{\rm c}P\widehat{A}_{\rm c}^T & \widetilde{F} - \widehat{A}_{\rm c}P\widehat{C}_{\rm c}^T \\ \widetilde{F}^T - \widehat{C}_{\rm c}P\widehat{A}_{\rm c}^T & \widetilde{E} - \widehat{C}_{\rm c}P\widehat{C}_{\rm c}^T \end{bmatrix} \geq 0, \quad P > 0 \tag{23}$$

where $\widetilde{H}(z) = \frac{\widetilde{E}}{2} + \widehat{C}_{\rm c}(zI_{n_x} - \widehat{A}_{\rm c})\widetilde{F}$.
4) Perform an SVD of $\widehat{\mathcal{M}}(\widetilde{E},\widetilde{F})$:

$$\widehat{\mathcal{M}}(\widetilde{E},\widetilde{F}) = \begin{bmatrix}\widetilde{U}_{n_e} & \widetilde{U}'_{n_e}\end{bmatrix} \begin{bmatrix} \Sigma_{n_e} & 0 \\ 0 & \Sigma'_{n_e} \end{bmatrix} \begin{bmatrix}\widetilde{U}_{n_e} & \widetilde{U}'_{n_e}\end{bmatrix}^T$$

where Σ_{n_e} contains the n_e largest singular values and define the estimates of B and D as

$$\begin{bmatrix} \widetilde{B} \\ \widetilde{D} \end{bmatrix} = \widetilde{U}_{n_e}\Sigma_{n_e}^{\frac{1}{2}}. \tag{24}$$

5) Set $\widehat{G}_x(z) = \widehat{C}_{\rm c}(zI - \widehat{A}_{\rm c})^{-1}\widetilde{B} + \widetilde{D}$.

A closely related subspace algorithm to ours was proposed in [15]. Since this algorithm uses unbiased auto-covariance estimates, it may yield a negative-definite auto-PSD estimate. The final step ensuring positive-definiteness of the estimated spectrum is identical to ours.

VI. Simulation Example

In this section, we use an academic example to illustrate the properties of Algorithms 5.1 and 5.2. This example will demonstrate the poor performance of the Welch estimators when used directly for the identification of auto-PSD and cross-PSD with closely spaced sharp peaks. But, the cross and auto-spectra will be identified accurately when the subspace algorithms are driven by the Welch estimators.

Let the transfer functions in Figure 1 be given by the state-space models:

$$\begin{aligned} G_x(z) &= C_x(zI - A_x)B_x + D_x, \\ G_y(z) &= C_y(zI - A_y)B_y + D_y, \\ H_x(z) &= \tilde{C}_x(zI - \tilde{A}_x)\tilde{B}_x + \tilde{D}_x, \\ H_y(z) &= \tilde{C}_y(zI - \tilde{A}_y)\tilde{B}_y + \tilde{D}_y \end{aligned}$$

where

$$A_x = \begin{bmatrix} -0.8 & 0.55 & 0 & 0 & 0 & 0 \\ -0.55 & -0.8 & 0 & 0 & 0 & 0 \\ 0 & 0 & 0.9 & 0.4 & 0 & 0 \\ 0 & 0 & -0.4 & 0.9 & 0 & 0 \\ 0 & 0 & 0 & 0 & -0.9 & 0.2 \\ 0 & 0 & 0 & 0 & -0.2 & -0.9 \end{bmatrix},$$

$$C_x = \begin{bmatrix} 1 & 1 & 0 & 1 & 0 & 0 \\ 0 & 1 & -1 & 1 & 0 & 3 \\ 0 & 0 & 0 & 1 & -1 & 0 \\ 0 & 1 & 0 & 0 & 0 & 0 \\ 0 & 0 & 1 & 0 & 0 & 0 \end{bmatrix},$$

$$B_x = \begin{bmatrix} 1 & 0 \\ 1 & 1 \\ 1 & 0 \\ 0 & 1 \\ 2 & -1 \\ 2 & 3 \end{bmatrix}, \quad D_x = \begin{bmatrix} 1 & 0 \\ -1 & 1 \\ 0 & 1 \\ 1 & 1 \\ 2 & 1 \end{bmatrix};$$

$$A_y = \begin{bmatrix} 0.8876 & 0.4494 & 0 & 0 \\ -0.4494 & 0.7978 & 0 & 0 \\ 0 & 0 & -0.6129 & 0.0645 \\ 0 & 0 & -6.4516 & -0.7419 \end{bmatrix},$$

$$B_y = \begin{bmatrix} 0 & 0 \\ 1 & 1 \\ 0 & -1 \\ -1 & 0 \end{bmatrix}, \quad D_y = \begin{bmatrix} 1 & 2 \end{bmatrix},$$

$$C_y = \begin{bmatrix} 1 & 0 & 3 & 0 \end{bmatrix};$$

$$\tilde{A}_x = \begin{bmatrix} 0.6 & 0.5 & 0 & 0 & 0 & 0 \\ -0.5 & -0.6 & 0 & 0 & 0 & 0 \\ 0 & 0 & 0.8 & 0.3 & 0 & 0 \\ 0 & 0 & -0.3 & 0.8 & 0 & 0 \\ 0 & 0 & 0 & 0 & 0.5 & 0 \\ 0 & 0 & 0 & 0 & 0 & -0.25 \end{bmatrix},$$

$$\tilde{C}_x = \begin{bmatrix} 3 & 1 & 0 & 5 & 1 & -1 \\ -1 & 0 & -1 & 2 & 1 & -3 \\ 1 & 2 & 3 & 0 & -1 & 1 \\ 0 & 0 & 7 & -1 & 0 & 2 \\ 1 & 1 & -5 & 0 & 3 & 1 \end{bmatrix},$$

$$\tilde{B}_x = \begin{bmatrix} 1 & 0 & -2 & 0 & 3 \\ 0 & 7 & 1 & 0 & 5 \\ 1 & -1 & 0 & 0 & 4 \\ -1 & -2 & 4 & 0 & 1 \\ 2 & -1 & 2 & 2 & 5 \\ 2 & 3 & -9 & 0 & 1 \end{bmatrix}, \quad \tilde{D}_x = I;$$

$$\tilde{A}_y = \begin{bmatrix} 0.6 & 0.4 & 0 & 0 \\ -0.4 & 0.6 & 0 & 0 \\ 0 & 0 & -0.5 & 0.5 \\ 0 & 0 & -0.5 & -0.5 \end{bmatrix},$$

$$\tilde{C}_y = \begin{bmatrix} 1 & -1 & 0 & 3 \end{bmatrix},$$

$$\tilde{B}_y = \begin{bmatrix} 0 \\ 1 \\ -1 \\ 5 \end{bmatrix}, \quad \tilde{D}_y = [1];$$

Note that $D_x \neq 0$ and $D_y \neq 0$. Likewise, in this example whether there exist finite zeros outside or on the unit circle is not our concern since we are not interested in determining the transfer functions in Eqs. (1) and (2). Our main concern is the accuracy of Algorithms 5.1 and 5.2.

To examine the accuracy of Algorithms 5.1 and 5.2, we performed Monte Carlo simulations estimating the cross-PSD matrix $S_{xy}(z)$ and the auto-PSD matrix $S_{xx}(z)$ of the above ARMAMA model from the data record: $x[k], y[k]$, $k = 0, \cdots, N-1$ by using different noise realizations and compared them with the Welch estimators in Eqs. (6) and (7). For $M = 16,384$ and $L = 256$, Algorithms 5.1 and 5.2 were used with $p = r = 200$. The quality of the models was assessed by determining the relative errors in the Frobenius norm defined for a given pair matrices X and Y of compatible sizes by

$$\rho(X, Y) = \frac{\|X - Y\|_F}{\|Y\|_F}. \tag{25}$$

In Figures 2 and 3, the results are shown for the estimators in Eqs. (7) and (21). We computed $\rho(\widehat{S}_{xy}^W, S_{xy}) = 0.6762$ and $\rho(\widehat{S}_{xy}, S_{xy}) = 0.0321$ with the latter denoting the relative error of Algorithm 5.1. Since $S_{xy}(e^{j\omega})$ and its estimates are matrix-valued functions of ω, it is reasonable to plot their largest and smallest nonzero singular values versus frequency. The latter is defined as the minimum of all singular values which do not vanish for all ω.

The Welch cross-PSD estimate appears to be drowned in noise and only some, not all, sharp peaks of the true cross-PSD are detectable from Figure 2. At other frequencies, scattering of the estimate resembles that of a white noise process and predicates the judgement about the poor performance of the Welch estimators. Nevertheless, Figure 2 contains also essential features of a spectral density, i.e., visible peaks. Then, Algorithm 5.1, owing to its interpolation property, from the Welch cross-PSD estimate recovers very accurately the true cross-PSD by averaging noise out in the Welch cross-PSD estimate as demonstrated in Figure 3.

Next, we study accuracy properties of Algorithm 5.2. This algorithm yielded $\rho(\widehat{S}_{xx}, S_{xx}) = 0.0600$ for a 12th order model with 7 inputs, and the parameters p and r were both set 200 as in Algorithm 5.1. The fit by this model is excellent as shown in Figure 4. The chosen model order is right since $G_x(z)$ and $H_x(z)$ are 6th order transfer matrices. The number of the inputs was determined from the singular value decomposition in step 4. This number

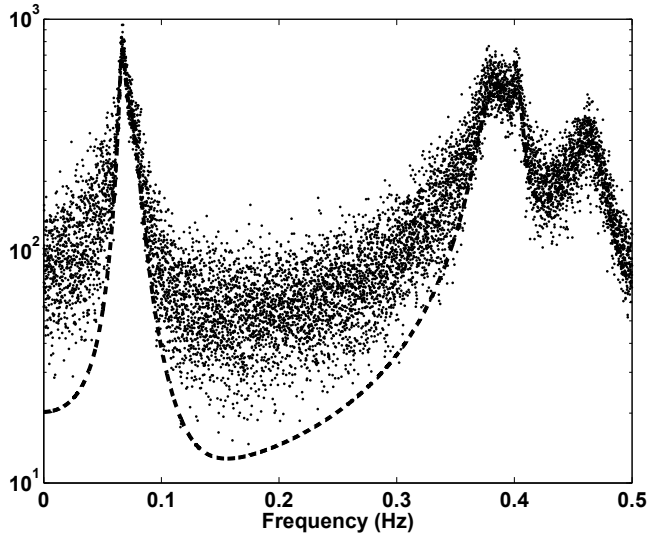

Fig. 2. the largest singular values of the true and the estimated cross-PSD matrices: (- -) the true cross-PSD; (·) the Welch cross-PSD estimate.

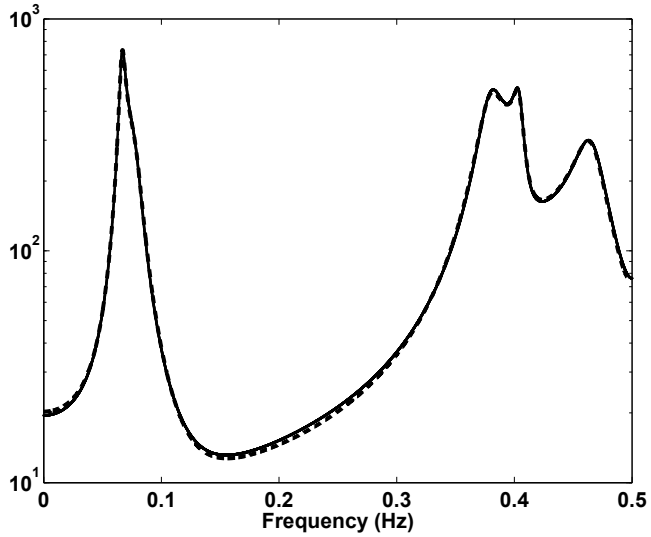

Fig. 3. the largest singular values of the true and the estimated cross-PSD matrices: (- -) the true cross-PSD; (·) the subspace estimate in Eq. (21).

is also right since $e[k] \in \mathbf{R}^2$ and $e_x[k] \in \mathbf{R}^5$. Thus, the identified spectral factor is a fat matrix with 7 inputs and 5 outputs. This identified spectral factor, however, can not be used to determine $G_x(z)$ and $H_x(z)$ since the correlation structure in the ARMAMA model described by Eqs. (1) and (2) was not considered explicitly. Steps 2 and 3 of Algorithm 5.2 were implemented since the auto-PSD estimates returned by Algorithm 5.2 were not positive real in all trials; thus, showing that steps 2 and 3 are effective in assuring non-negativity of the estimated spectrum. Due to space limitations, the results for the Welch auto-PSD estimator in Eq. (6) were omitted.

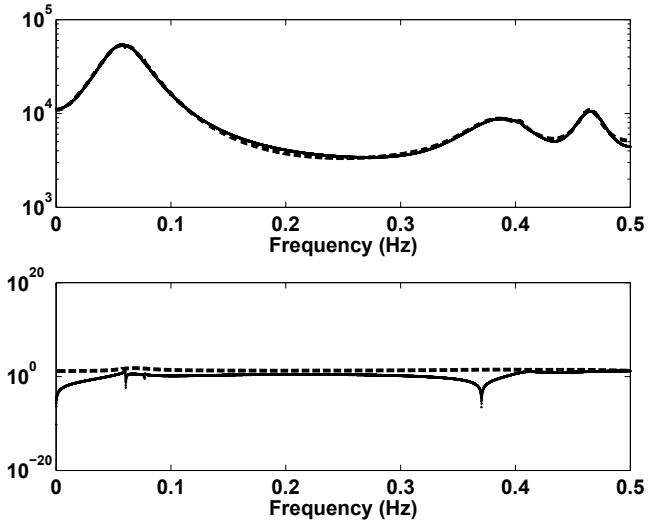

Fig. 4. the largest and the smallest nonzero singular values of the true auto-PSD matrix of x and the 12 th order subspace estimate with 7 inputs returned by Algorithm 5.2: (- -) the true auto-PSD; $(\cdot)$ the subspace estimate.

VII. An application to modeling of acoustic spectra

In a fault detection study, experiments were carried out on both healthy and faulty induction motors. The fault types studied were ball bearing failures and eccentricities, broken rotor cage bars, short circuits in the stator windings. The experiments were performed in a reverberant and noisy room to simulate the real working environment. Each experiment was repeated twice. An array of five microphones of the same type with the frequency band 20Hz–20kHz were hemispherically placed around the motors. The microphones were connected to an amplifier and professional sound card unit and sampled at the rate 44.1 kHz about 30 seconds for each experiment. The measurements were recorded after the motors reached the steady state. The motors were coupled to a single phase generator with permanent magnet, which provided loads varying between 3.8 and 5.4 Amperes. The test rig used in the experiments is shown in Figure 5.

For each experiment, the data were divided equally into the two disjoints sets: the estimation and the validation data sets. Then, the Welch auto-PSD estimate in Eq. (6) was calculated for $M = 1000$ on both data sets. In Figure 6, the largest and the smallest nonzero singular values of the five-microphone array Welch auto-PSD estimate of a healthy motor are plotted for both the estimation and the validation data sets. The motor was partially loaded and the current drawn was minimum, i.e., 3.8 Amperes.

In Figure 7, for the healthy motor in Figure 6, the largest and the smallest singular values of the auto-PSD matrix of the five-microphone array estimated by Eq. (6) with parameters $M = 1000$ and $L = 480$ and Algorithm 5.1 with the parameter values $p = r = 200$ and the 35th order model using the estimation data only are plotted versus frequency. The fit by the subspace algorithm is impressive in spite of many spikes in the data. None of the spikes are missed

Fig. 5. the test rig.

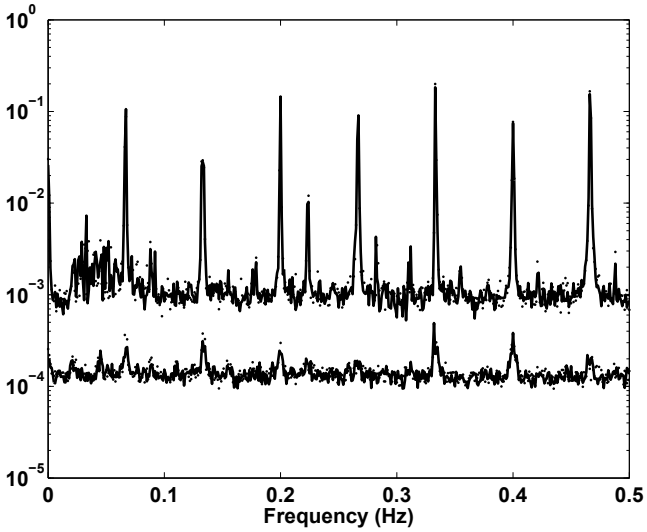

Fig. 6. the largest and the smallest singular values of the five-microphone array Welch auto-PSD estimate of a healthy electric motor for $L = 480$: (–) estimation data; $(\cdot)$ validation data.

by Algorithm 5.1. The off-diagonal entries of the estimated cross-PSD matrix are the cross-PSD function estimates of the microphone pairs in the array, and the diagonal entries are the auto-PSD function estimates of the individual microphones.

It was not possible to extract the spectral factor of the subspace estimate plotted in Figure 7 since the estimated poles were very close to the unit circle. In fact, for the healthy motor plotted in Figures 6 and 7 the first microphone of the array using the estimation data only and the parameter values chosen as before, we found that the poles of the estimated auto-PSD were almost on the unit circle with a distance 1.5×10^{-7} to it and the farthest away pole from the unit circle had a modulus 0.969. Moreover, the power spectrum estimate had a minimum value of -0.0081. These values explain the difficulty faced in computing a spectral factor even for a scalar spectrum. This is an example to auto-regressive moving-average modeling of harmonic signals.

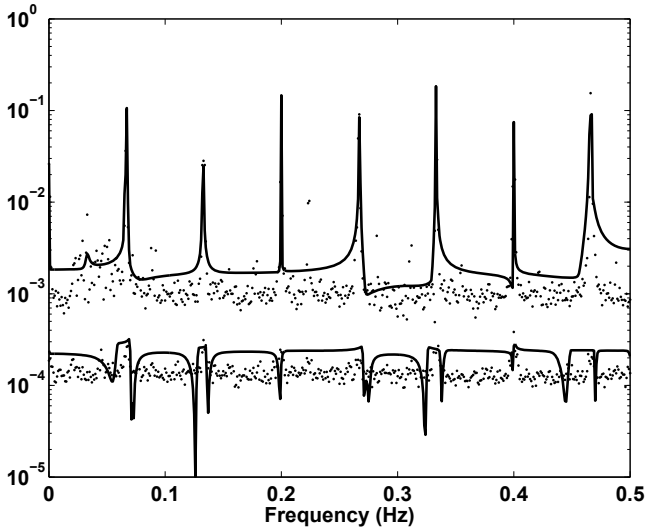

Fig. 7. the cross-PSD magnitudes of the 5-microphone array estimated by the Welch method and the subspace algorithm for the healthy motor and $M = 1000$, $L = 480$, $p = r = 200$ using the estimation data only : $(\cdot)$ the Welch cross-PSD estimate; (–) Algorithm 5.1 with a 35th order model.

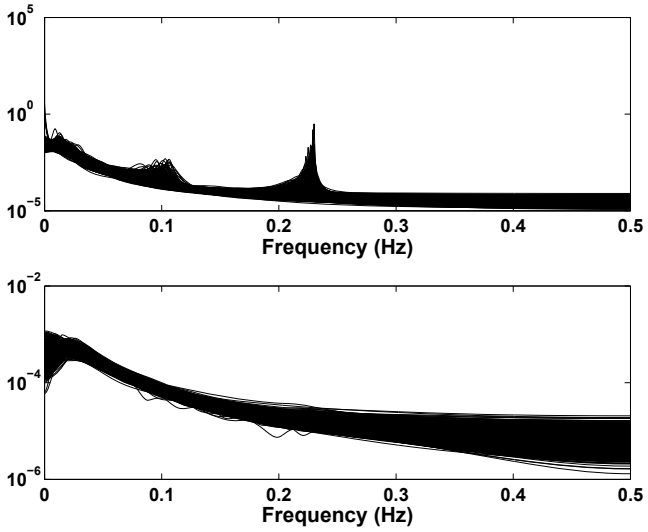

Fig. 8. the largest and the smallest singular values of the five-microphone array auto-PSD matrix estimated by the N4SID algorithm with $M = 1000$ and over 480 trials for the healthy motor plotted in Figures 6 and 7.

Although, in this example, we were not able to extract spectral factors directly from the auto-PSD estimates, we were, however, able to accurately identify their eigenstructures by utilizing the cross-spectral analysis. In structural vibration monitoring, a plethora of fault detection methods is based on monitoring changes in eigenstructures [16].

We end this section by studying the performance of the N4SID algorithm on the acoustic data. The time-domain measurements used to obtain the identification results plotted in Figures 6 and 7 were used to compute the spectral estimate by the N4SID algorithm. In Figure 8, the estimation results are shown for 480 trials. In each trial, 1000 measurements were used, and the N4SID algorithm picked the best model order. As expected, due to the implementation of the positive-realness constraint, the N4SID algorithm has failed.

VIII. Conclusions

In this paper, properties of two subspace-based identification algorithms recently developed in [10] to estimate the cross-PSD and the auto-PSD matrices from sampled values of the Welch cross and auto-PSD estimators on uniform grids of frequencies were illustrated in a case study by using academic and real-life application examples. Preliminary results indicate good performance of the proposed algorithms.

Acknowledgment

The authors would like to thank Prof. E. Germen for providing them with the measured acoustic data used for testing the identification algorithms.

References

[1] C. H. Knapp and G. C. Carter, "The generalized correlation method for estimation of time delay," *IEEE Trans. Acoust., Speech, Signal Processing*, vol. ASSP-30, pp. 320–327, 1976.

[2] G. C. Carter, *Coherence and Time Delay Estimation*, Piscataway,NJ: IEEE Press, 1993.

[3] H. Pozidis and A. P. Petropulu, "Cross-spectrum based blind channel identification," *IEEE Tr. Signal Proc.*, vol. 45, pp. 2977–2992, 1997.

[4] M. Rahmani, A. Akbari, B. Ayad, B. Lithgow, "Noise cross PSD estimation using phase information in diffuse noise field," *Signal Processing*, vol. 89, pp. 703–709, 2009.

[5] H. Akaike, "Some problems in the application of the cross-spectral method," in: B. Harris (Ed.), Spectral Analysis of Time Series, John Wiley, 1967, pp. 81–107

[6] M. J. Schulz, P. F. Pai, A. S. Naser, S. K. Thyagarajan, G. J. Brannon, and J. Chung, "Locating structural damage using frequency response reference functions and curvatures," in: *Proc. Int. Workshop Structural Health Monitoring*, Stanford University, pages 690–701, 1997.

[7] H. A. Panofsky, "Meteorological applications of cross-spectrum analysis," in: *Proc. Advanced Seminar Conducted by the Mathematical Research Center*, pages 109–132, 1996.

[8] K. Kanazawa, "Application of cross spectrum based modal identification to output-only records of ambient vibration," in: *Proc. 13th World Conf. Earthquake Engineering*, Vancouver, B. C., Canada, paper no 3068, August 2004.

[9] K. Kanazawa and K. Hirata, "Parametric estimation of the cross-power spectral density," *J. Sound Vibr.*, vol. 282, pp. 1–35, 2005.

[10] H. Akçay, "Estimation of cross-power and auto-power spectral densities in frequency domain by subspace methods," in: *Proc. 51st IEEE CDC*, Maui, HI, December 2012, pages 3445–3450.

[11] G. Picci and S. Pinzoni, Dynamic Factor-Analysis models for stationary processes, IMA Journal on Mathematics of Control and Information, Vol.3, No. 2 , pp. 185–210, 1986.

[12] M. Deistler and C. Zinner, Modelling high-dimensional time series by generalized linear dynamic factor models: An Introductory survey, Communications in Information and Systems, vol. 7, no. 2, pp. 153-0166, 2007.

[13] C. T. Chou and M. Verhaegen, Subspace algorithms for the identification of multivariable dynamic errors-in-variables models, Automatica, pp. 1857-1869, 1997.

[14] P. D. Welch, "The use of fast Fourier transform for the estimation of power spectra," *IEEE Trans. Audio Electroacoust.,* vol. AU-15, pp. 70–73, 1967.

[15] T. McKelvey, H. Atala, and D. O. Blanco Parada, A subspace method for frequency selective identification of stochastic systems, in: Proceedings of the 17th World Congress IFAC, Seoul, Korea, pages 8846–8851, July 2008.

[16] M. Basseville, M. Abdelghani, and A. Benveniste, "Subspace-based fault detection algorithms for vibration monitoring," *Automatica*, vol. 36, pp. 101–109, 2000.